Korean J. Chem. Eng., **30**(9), 1710-1715 (2013)
DOI: 10.1007/s11814-013-0119-3

An evaluation of trimethyl phosphate on deactivation of Cu/Zn catalyst in hydrogenation of dodecyl methyl ester

Hui Huang*,, Guiping Cao**,†, and Shaohong Wang*****

*School of Chemical Engineering, Ningbo University of Technology, Ningbo 315016, China
**UNILAB, State Key Lab of Chemical Engineering, East China University of Science and Technology, Shanghai 200237, China
***Shanghai Huayi Group Co., Ltd., Shanghai 200431, China
(*Received 31 January 2013 • accepted 3 July 2013*)

Abstract−The effect of trimethyl phosphate on Cu/Zn catalyst prepared by co-precipitation method for hydrogenation of methyl laurate to dodecanol in a slurry phase was studied using a stirred autoclave reactor system. The catalysts were characterized by means of XRD, EDS, XPS, SEM and BET. The results indicated that catalytic activity decreased with the increased amount of trimethyl phosphate. Correlating with the results from the above characterization, it was found that the main cause for the catalyst deactivation was the trimethyl phosphate occlusion of active sites by the physical adsorption and BET surface area decrement.

Key words: Fatty Alcohol, Cu/Zn Catalyst, Deactivation, Phosphate

INTRODUCTION

Fatty alcohols (FOH) are a kind of non ionic surfactant due to their amphipathic nature, and find application in emulsifiers, emollients, as well as thickeners in cosmetics and food industries. Their derivatives are widely used as surfactants, lubricants, or additives in many industrial products [1,2]. FOH constitute one of the largest groups of the oleochemicals. Commercially, fatty alcohols are produced by one of the following three processes: Ziegler process, Oxo process, or catalytic hydrogenation of fatty acids or esters. The Ziegler process is based on long-chain trialkyl aluminum derivatives hydrolysis, yielded by metallic aluminum, hydrogen, and triethyl aluminum reaction in the presence of ethylene. The Oxo process consists of a reaction of olefins with a H_2/CO gas mixture in the presence of a suitable catalyst. The hydrogenation process is the only process that uses natural fats or oils as raw material, whereas the other two processes utilize petrochemicals feedstocks instead [3-5]. To ensure a high degree of product safety to consumers (especially for food and cosmetic related products) and the environment, renewable resources are preferential to petrochemical raw materials, and therefore are regarded as ideal feedstocks for FOH production.

In the hydrogenation of fatty esters to produce FOH, copper-based catalysts are selected for their intermediate catalytic activity for hydrogenation reactions. Cu exhibits high selectivity for esters hydrogenation toward alcohols, rather than total hydrogenation to the corresponding alkanes. Copper-based catalysts can be tracked back to as early as the 1930's, when copper-chromium (Cu/Cr) catalyst was developed for hydrogenation of ethyl ester [6]. Similar catalysts are still frequently used today for hydrogenation of fatty esters [7-9]. Nowadays, chromium-containing catalysts are believed to be toxic and detrimental to irrigation systems and soil, due to the releasing of environmentally hazardous Cr^{6+} in the Cu/Cr catalyst preparation and use. Research has therefore been focused on the replacement of chromium by transition metals, such as zinc [10], manganese [11,12], iron [13] and other greener promoters [14,15]. Cu/Zn catalysts are recognized as ideal substitute for Cu/Cr catalysts among others, from which the profound effect of zinc and the synergistic effect between copper and zinc could be expected [10], as well as its specific catalyst structure [16]. Grunwaldt and co-workers have conducted *in situ* studies of Cu/Zn catalysts under reductive atmosphere; it is shown by means of extended X-ray fine structure spectroscopy (EXAFS) that metallic zinc will partially dissolve in copper to promote activities of Cu [17]. On the other hand, the stability of Cu/Zn catalyst is compromised by reaction conditions and substrates with respect to Cu/Cr system. It is desirable to understand the various parameters that affect the stability of Cu/Zn catalyst in commercial processes.

As far as raw materials are concerned, natural oils, such as coconut oil and palm kernel oil, are among the best options of the feed stocks for FOH production, which however, always contain impurities that are harmful for the catalyst and are difficult to separate from fatty esters. Examples of catalyst poisons or inhibitors could be water, soaps, fatty acids, glycerin, glycerides and sodium [4,18-20]. Some of the impurities are introduced during plant growing, while others originate from pesticides, or fatty ester preparations [3, 21]. Even traces of these impurities (ppm levels) in the feedstock may act as reaction inhibitors or catalyst poisons, which would cause catalyst deactivation and shorten the life time of the catalyst. In the commercial process of FOH production, for instance, the life time of mostly used Cu/Zn catalyst is only about 3 to 6 months. Among these molecules that deactivate Cu/Zn catalyst, some molecules cover the active sites and inhibit substrates from approaching to cause temporary loss of activities. These inhibitors can be washed off to restore the activity of fresh catalyst. For example, we have shown that water is an inhibitor in hydrogenation of dodecyl methyl esters [22], and

†To whom correspondence should be addressed.
E-mail: gpcao@ecust.edu.cn

Thakur and co-workers [18] have shown that glycerine and monoglyceride could inhibit active sites during dodecyl methyl ester hydrogenation. While some impurities, such as chlorine species, could cause perpetual lose of activity and need to be removed from feedstocks pretreatment [23]. The measures to prevent both inhibition and permanent deactivation rely on causes or the nature of deactivation.

Presently, little is reported in literature on the nature of the phosphate compounds present in fatty methyl esters prepared from natural fats or oils; possible candidates are degradation products of phosphor-containing proteins or pesticides and phosphorous compounds in boiler water from the pretreatment process [4,21], and typical concentrations of phosphorous compounds present in fatty methyl esters prepared from natural fats or oils are over 10 mg/kg [24]. Quinn et al. [25] have evaluated PH_3 as methanol synthesis catalyst poisons; reaction of metallic copper with phosphine was suggested for the extremely favorable equilibrium constant. However, no distinct bulk copper phosphide or phosphate phases are further corroborated by limited characterization methods. Literature reports on this topic are rather scarce, probably for commercial reasons. Controversy still hangs over the effect of phosphor-containing compounds on the Cu/Zn catalyst.

Herein, we present deactivation studies of trimethyl phosphate during hydrogenation of dodecyl methyl ester, targeted at gaining an understanding of the effects of organophosphorous compound on the Cu/Zn catalyst prepared by co-precipitation method. This knowledge is desirable to improve the performance of commercial catalysts for hydrogenation of fatty acid methyl ester (FAME) to FOH. The hydrogenation of dodecyl methyl ester to dodecanol is taken as a model reaction, and the conditions are close to industrial performances.

EXPERIMENTAL

1. Catalyst Preparation

The Cu/Zn catalyst was prepared by parallel co-precipitation method according to our preceding paper [22]. Mole ratio of Cu : Zn for the final synthesis catalyst was 1.5. After dissolving 21.75 g $Cu(NO_3)_2 \cdot 3H_2O$ and 17.85 g $Zn(NO_3)_2 \cdot 6H_2O$ in 500 ml of de-ionized water, 200 ml of aqueous solution of 19 g Na_2CO_3 was added under vigorous stirring at 50 °C. The obtained precipitate was washed repeatedly with de-ionized water after the filtration of the suspension. After drying at 110 °C overnight, the solid was crushed and pelleted by adding 2 wt% of graphite. The pellet was reduced under 10 ml/min of hydrogen by heating to 240 °C at a rate of 5 °C/h and then cooled to room temperature under hydrogen. The fresh catalyst was transferred in nitrogen atmosphere and stored in dodecyl methyl ester before use.

2. Catalytic Reactions

Catalyst deactivation measurements were made in a 1-L stirred batch reactor. Catalytic tests were typically run by charging the reactor with about 400 g catalyst/ester slurry with a weight ratio of 0.025 and various amount of trimethyl phosphate, followed by raising the hydrogen pressure to about 4 MPa. The reactor temperature was then raised to 240 °C and the hydrogen pressure was increased to 21 MPa. After reaction of a controlled time, the reactor was cooled to room temperature and the gas was vented. Liquid samples were analyzed by a gas chromatograph (GC) equipped with a flame ionization detector (FID). 1-Octanol was used as the internal standard compound for analysis. All reactants were identified by Micromass GCTTM GC-mass spectroscopy.

The reaction equation can be generalized according to:

$$C_{11}H_{23}\text{-}COOCH_3+2H_2 \rightarrow C_{11}H_{23}\text{-}CH_2OH+CH_3OH \quad (1)$$

In addition to the main reaction, there was an important side reaction. Transesterification products were intermediates and the formation was favored by the presence of the product alcohol [10]:

$$C_{11}H_{23}\text{-}COOCH_3+C_{11}H_{23}\text{-}CH_2OH \rightarrow C_{11}H_{23}\text{-}COOCH_2\text{-}C_{11}H_{23}+CH_3OH \quad (2)$$

3. Catalyst Characterization

Powder X-ray diffraction (XRD) patterns were recorded using a Rigaku D/Max 2550 VB/PC diffractometer (Japan) equipped with Cu/Kα (λ=0.154056 nm) radiation operating at 40 kV and 450 mA for 2θ angles ranging from 10° to 80° at a step of 8°/min. The spent catalyst after reaction was immersed from oxidation in benzene and polystyrene.

Elemental composition was determined by FALCON X-ray energy dispersive spectroscopy (EDS, an EDAX spectrometer) with a 15 kV acceleration voltage.

The surface chemical composition was analyzed with XPS by use of a Kratos AXIS ULTRA X-ray photoelectron spectrometer (Kratos Analytical, Manchester, U.K.). The XPS spectra were recorded in the fixed analyzer transmission mode with a Al Kα (1,486.7 eV) X-ray source operated at 150 W (15 kV/10 mA), and the binding energy values were obtained with reference to the C 1s peak from the carbon surface deposit at 284.6 eV. The samples were analyzed in an analytic chamber at pressures below 1.33×10^{-7} Pa.

The nitrogen adsorption-desorption isotherms were measured on a Micromeritics ASAP 2010 chemisorption analyzer (USA). The samples were degassed at 190 °C for 6 h to obtain a residual pressure of less than 10^{-5} Torr. The surface area was determined by adsorption-desorption of nitrogen at 77 K. The pore volume and average pore diameter were calculated by the BET method. The pore-diameter distributions were calculated by using the BJH method on the desorption branch.

SEM images were acquired in a JEOL JSM-6700F scanning electron microscope (Japan) operated at 15 kV.

RESULTS AND DISCUSSION

1. Effect of Trimethyl Phosphate on the Catalytic Performance of Cu/Zn Catalyst

Varied amounts of trimethyl phosphate are added in hydrogenation of dodecyl methyl ester for investigating the influence of trimethyl phosphate on the catalytic activity of the Cu/Zn catalyst. In Fig. 1, the conversion of dodecyl methyl ester and selectivity towards dodecanol as a function of the trimethyl phosphate concentration are displayed. It is clear that the poisoned catalysts deactivate rapidly and show both inferior activity and selectivity in the hydrogenation of dodecyl methyl ester to dodecanol; e.g., when the concentration of trimethyl phosphate is increased from 0 to 0.5 mmol/$g_{catalyst}$, the conversion decreases from 97% to 54%, and the selectivity decreases from 96% to 56%. No catalytic activity is observed at the concen-

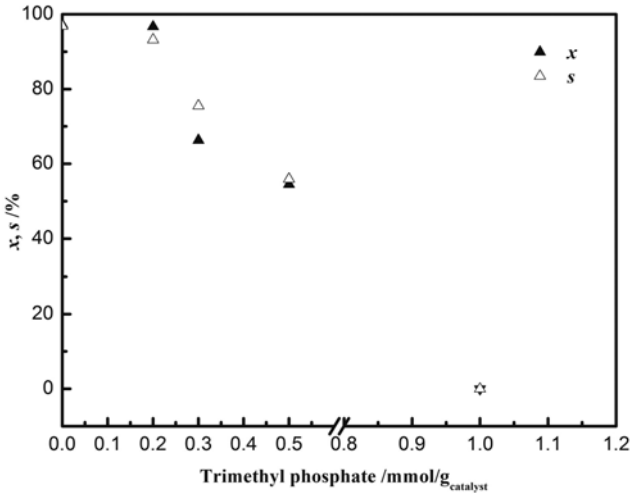

Fig. 1. Conversion of methyl laurate and selectivity of dodecanol versus trimethyl phosphate concentration (reaction conditions: Cu/Zn catalyst, $m_{catalyst}/m_{methyl\ laurate}$=0.025, T=240 °C, P=21 MPa, t=5 h, n=750 rpm).

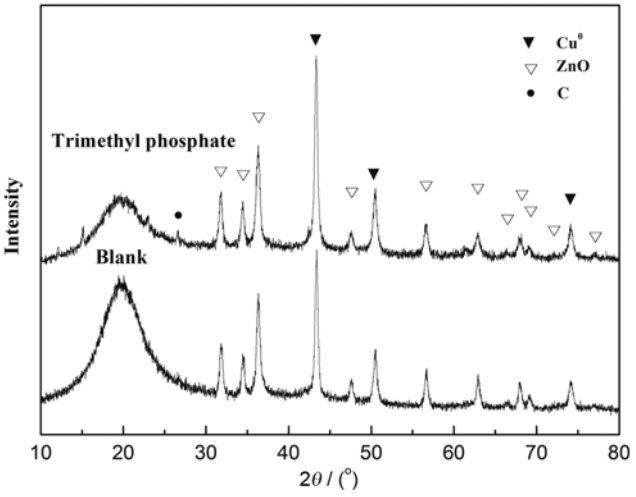

Fig. 2. XRD patterns of the Cu/Zn catalysts: (1) after reaction without adding trimethyl phosphate; (2) after reaction with adding 0.5 mmol/$g_{catalyst}$ of trimethyl phosphate in methyl laurate.

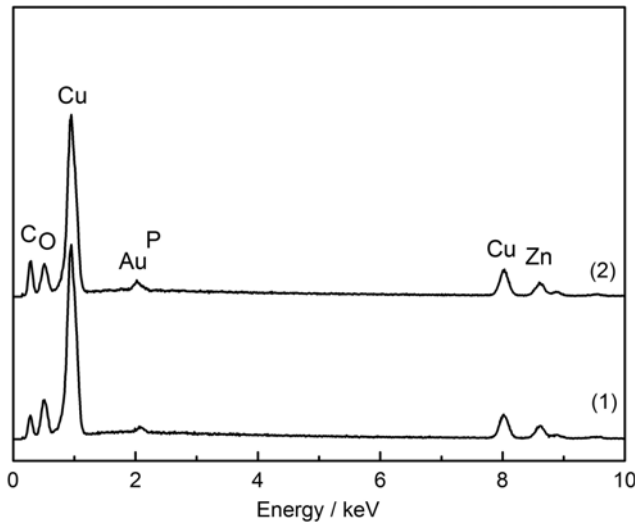

Fig. 3. EDS of Cu/Zn catalysts: (1) blank; (2) deactivated by 0.5 mmol/$g_{catalyst}$ trimethyl phosphate.

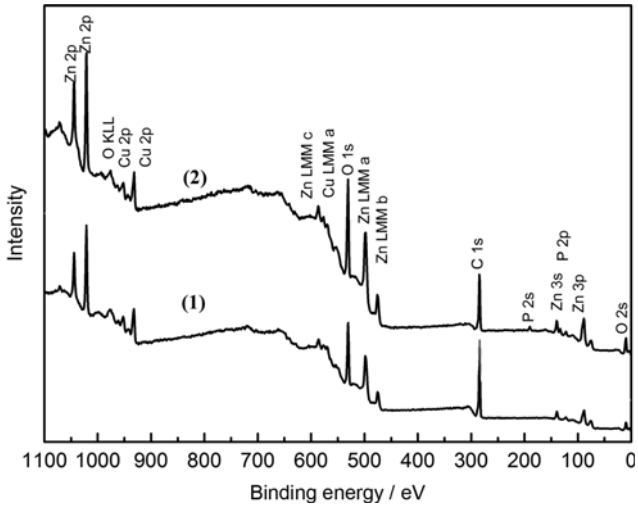

Fig. 4. XPS patterns of Cu/Zn catalysts: (1) blank; (2) deactivated by 0.5 mmol/$g_{catalyst}$ trimethyl phosphate.

tration of 1.0 mmol/$g_{catalyst}$.

2. Characterization of Catalysts

XRD patterns of Cu/Zn catalyst samples are shown in Fig. 2. Distinct diffraction peaks in Fig. 2 are assigned to Cu^0 (PDF#65-9026), ZnO (PDF#36-1451) and C (PDF#65-6212), appearing at 2θ=43.3°, 50.5°, 74.2°; 31.8°, 34.4°, 36.3°, 47.5°, 56.6°, 62.9°, 66.4°, 68.0°, 69.1°, 72.6°, 77.0°; 26.5°, respectively. XRD patterns indicated that no new compounds were found on the catalyst after trimethyl phosphate deactivation and trimethyl phosphate had no influence on the valence state of the catalytic active site.

The absence of phosphate in Fig. 2 may be attributed to the physical adsorption or nonexistence of phosphate on the catalyst. EDS was characterized to confirm whether phosphor existed on the catalyst or not. As shown in Fig. 3, Cu, Zn and O were observed, due to the Cu^0 and ZnO, C and Au were attributed to the graphite addition in catalyst preparation and sample preparation before characterization, respectively. It can also be seen from Fig. 3 that P newly appeared on the Cu/Zn catalyst deactivated by trimethyl phosphate, when compared with the blank one. It is inferred from the XRD and EDS results that organophosphorous compound existed on the Cu/Zn catalyst, in the physical adsorbed form.

For further understanding of the nature of physisorbed phosphoric species, XPS measurement was conducted. Fig. 4 shows a survey scan for the surface of Cu/Zn catalysts. Peaks corresponding to

Table 1. Surface composition of Cu/Zn catalysts obtained from XPS

Catalysts	Atomic concentration, %				
	Cu	Zn	C	O	P
No trimethyl phosphate	18.34	20.06	23.79	37.81	0
0.5 mmol/$g_{catalyst}$ trimethyl phosphate	4.90	11.33	45.64	35.48	2.65

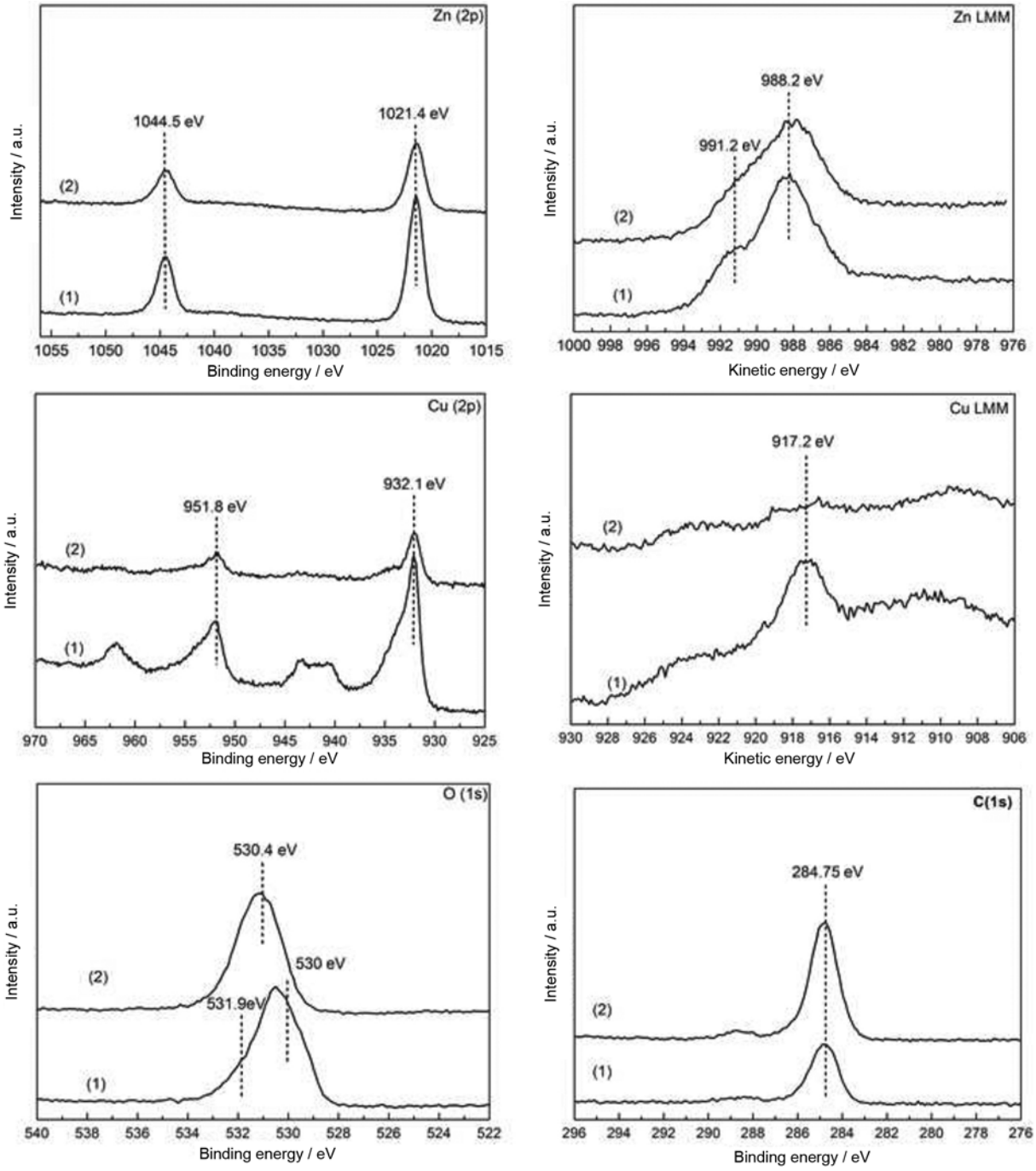

Fig. 5. X-ray photoelectron spectra of surface of Cu/Zn catalysts showing the Zn (2p), Zn (LMM), Cu (2p), Cu (LMM), C (1s) and O (1s) regions: (1) blank test; (2) deactivated by 0.5 mmol/$g_{catalyst}$ trimethyl phosphate.

Zn, Cu, C, O and P, along with their corresponding Auger peaks are clearly evident, which justified the existence of P on the trimethyl phosphate deactivated Cu/Zn catalyst. The surface composition data obtained from XPS is listed in Table 1; the atomic concentration of C and P increases from 23.79% and 0% to 45.64% and 2.65%, respectively, showing the evidence of trimethyl phosphate at the catalyst surface. The decrement in the atomic concentration of Cu and Zn is believed to be caused by occlusion of trimethyl phosphate. The Zn (2p), Zn (LMM), Cu (2p), Cu (LMM), C (1s) and O (1s) spectral regions are shown in Fig. 5. From the Zn $2p_{3/2}$ and Zn LMM spectrum, it is inferred that the surface of two catalysts consists of Zn^{2+}. As the Cu $2p_{3/2}$ core level and Cu LMM Auger spectra depicted, strong satellite peak on the higher BE side above 940 eV suggested the existence of Cu^{2+} at the surface of Cu/Zn catalyst marked as (1) [26]; this may due to the surface oxidation before XPS characterization. The Cu 2p spectrum contains a peak near 932.4 eV, which is characteristic of either Cu^0 or Cu^{1+}. The Auger spectrum is, in fact, very useful to distinguish between Cu^{1+} and Cu^0 as they differ in their KE, but display the same BE in core level results. The Cu Auger spectra of the catalyst, marked as (1), shows

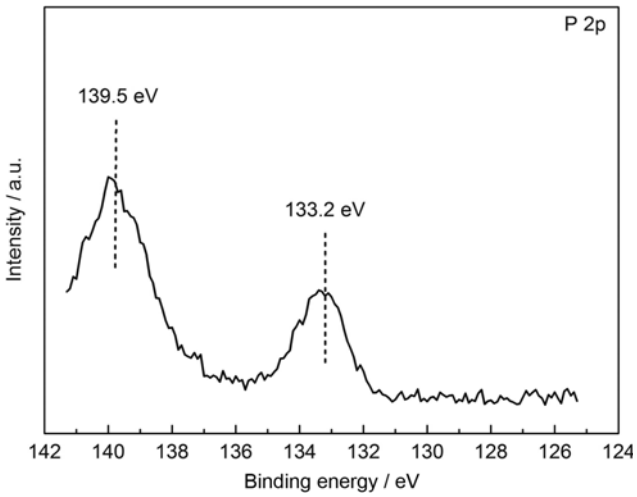

Fig. 6. X-ray photoelectron spectra for the P (2p) region of the surface of Cu/Zn catalysts deactivated by 0.5 mmol/$g_{catalyst}$ trimethyl phosphate.

a sharp peak at 917.2 eV with α'=1,849.6 eV. These parameters are very close to that of Cu metal [27,28], indicating that Cu^0 clusters are present on the catalyst surface.

By comparison of the C (1s) peaks, the peak of 284.75 eV is characteristic of graphite [29]. The O (1s) spectrum consists of peaks related to O^{2-} in the ZnO lattice (530.4 eV or 531.2 eV), surface hydroxyl groups (531.9 eV) [30,31].

Fig. 6 shows the XPS spectra of P 2p regions of the surface of Cu/Zn catalyst deactivated by 0.5 mmol/$g_{catalyst}$ trimethyl phosphate. As shown in Fig. 6, the P (2p) line has two peaks, 133.2 eV and 139.5 eV, and those high binding energies could be interpreted as surface P^{5+}, probably in the form of phosphates [32].

The morphology of the surface particles of Cu/Zn catalyst samples is shown in Fig. 7. As shown in Table 2, all catalysts share the similar average particle size (40.05±1.51 nm), and no obvious particle size change is observed from the used catalysts with increment of trimethyl phosphate in methyl laurate, suggesting that trimethyl phosphate has minor effect on the particle size of the Cu/Zn catalyst. However, it can also seen from Fig. 7 that there is an apparent

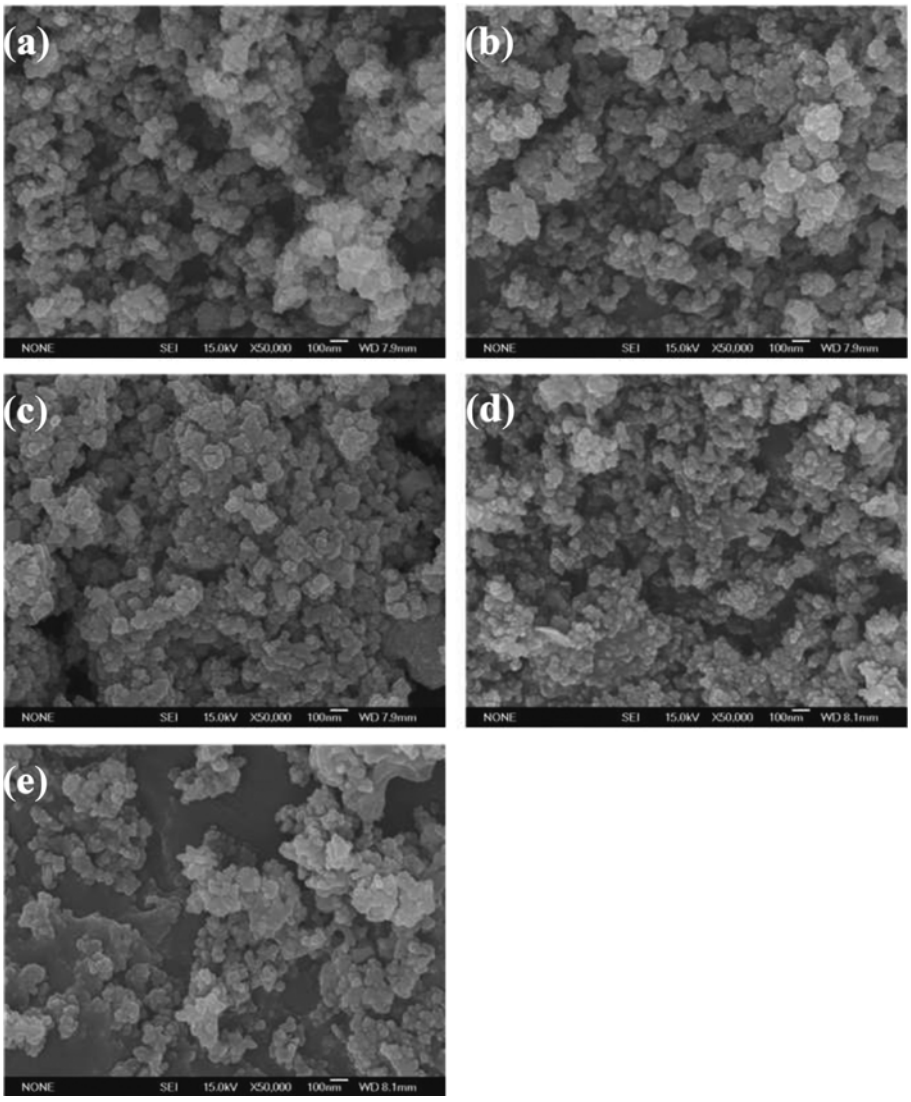

Fig. 7. SEM of Cu/Zn catalysts deactivated by: (a) no trimethyl phosphate; (b) 0.2 mmol/$g_{catalyst}$ trimethyl phosphate; (c) 0.3 mmol/$g_{catalyst}$ trimethyl phosphate; (d) 0.5 mmol/$g_{catalyst}$ trimethyl phosphate; (e) 1.0 mmol/$g_{catalyst}$ trimethyl phosphate.

Table 2. Physical properties of Cu/Zn catalysts

Catalysts	S_{BET} m^2/g	Pore volume ml/g	Average pore diameter nm	Average particle size nm
No trimethyl phosphate	19.1	0.11	12.30	41.16
0.2 mmol/$g_{catalyst}$ trimethyl phosphate	17.11	0.08	22.94	39.30
0.3 mmol/$g_{catalyst}$ trimethyl phosphate	15.59	0.07	23.24	41.56
0.5 mmol/$g_{catalyst}$ trimethyl phosphate	14.48	0.06	26.75	38.53
1.0 mmol/$g_{catalyst}$ trimethyl phosphate	11.93	0.04	32.36	41.26

difference between the background of the Cu/Zn catalyst deactivated by 1.0 mmol/$g_{catalyst}$ trimethyl phosphate and the other four, this probably is attributed to the complete catalytic activity loss as shown in Fig. 1.

The textural properties of the Cu/Zn catalysts are also listed in Table 2. BET surface area of the Cu/Zn catalyst samples varied with the amount of trimethyl phosphate in methyl laurate. It is found that the variation of surface area has the same trend with that of the Cu/Zn catalytic activity in Fig. 1, and the BET surface area decreases with the increment of trimethyl phosphate in methyl laurate, indicating that the surface area has a significant effect on the catalytic performance in the present case. From correlation with EDS, XPS and SEM results, it is suggested that the increment of physically adsorbed trimethyl phosphate causes the decrement of BET surface area and pore volume of the Cu/Zn catalysts and the blockage of the small pore results in the increment of the average pore diameters.

CONCLUSIONS

The effect of trimethyl phosphate on the hydrogenation of methyl laurate to dodecanol over Cu/Zn catalyst was evaluated in a stirred autoclave reactor. The results indicate that the negative effect on catalytic activity becomes more serious with the increment of trimethyl phosphate in methyl laurate, ranging from 0 to 0.5 mmol/$g_{catalyst}$. According to XRD, EDS, SEM, XPS and BET characterization results, it is believed that trimethyl phosphate existed in the methyl laurate could physically adsorb on the Cu/Zn catalyst and decreased the BET surface area by occlusion of active sites, leading to the rapid deactivation of the Cu/Zn catalyst.

ACKNOWLEDGEMENTS

This work is financially supported by Shanghai Huayi (Group) Company, Shanghai Zhongyuan Chemical Company Ltd. and K.C. Wong Education (Hong Kong).

REFERENCES

1. D. Myers, *Surfactant science and technology*, John Wiley & Sons, New York (2006).
2. C. Huang, H. Zhang, Y. Zhao, S. Chen and Z. Liu, *J. Colloid Interface Sci.*, **386**, 60 (2012).
3. U. K. Kreutzer, *J. Am. Oil Chem. Soc.*, **61**, 343 (1983).
4. T. Voeste and H. Buchold, *J. Am. Oil Chem. Soc.*, **61**, 350 (1984).
5. E. Leonard, *J. Am. Oil Chem. Soc.*, **60**, 1160 (1983).
6. H. Adkins and R. Connor, *J. Am. Chem. Soc.*, **53**, 1091 (1931).
7. T. Turek, D. L. Trimm and N. W. Cant, *Catal. Rev.*, **36**, 645 (1994).
8. R. Rieke, D. Thakur, B. Roberts and G. White, *J. Am. Oil Chem. Soc.*, **74**, 341 (1997).
9. R. Rieke, D. Thakur, B. Roberts and G. White, *J. Am. Oil Chem. Soc.*, **74**, 333 (1997).
10. F. T. van de Scheur and L. H. Staal, *Appl. Catal. A*, **108**, 63 (1994).
11. D. S. Brands, E. K. Poels, T. A. Krieger, O. V. Makarova, C. Weber, S. Veer and A. Bliek, *Catal. Lett.*, **36**, 175 (1996).
12. D. S. Brands, E. K. Poels and A. Bliek, *Stud. Surf. Sci. Catal.*, **101**, 1085 (1996).
13. Y. Hattori, K. Yamamoto, J. Kaita, M. Matsuda and S. Yamada, *J. Am. Oil Chem. Soc.*, **77**, 1283 (2000).
14. D. S. Brands, E. K. Poels and A. Bliek, *Appl. Catal. A*, **184**, 279 (1999).
15. Y. Z. Chen and C. L. Chang, *Catal. Lett.*, **48**, 101 (1997).
16. K. Tohji, Y. Udagawa, T. Mizushima and A. Ueno, *J. Phys. Chem.*, **89**, 5671 (1985).
17. J. D. Grunwaldt, A. M. Molenbroek, N. Y. Topsoe, H. Topsoe and B. S. Clausen, *J. Catal.*, **194**, 452 (2000).
18. D. Thakur, B. Roberts, G. White and R. Rieke, *J. Am. Oil Chem. Soc.*, **76**, 995 (1999).
19. F. T. van de Scheur, G. Sai and L. H. Staal, *J. Am. Oil Chem. Soc.*, **72**, 1027 (1995).
20. K. W. Jun, W. J. Shen, K. S. R. Rao and K. W. Lee, *Appl. Catal. A*, **174**, 231 (1998).
21. P. B. Guan, *Manufacture and application of fatty alcohol*, China Light Industry Press, Beijing (1990).
22. H. Huang, G. P. Cao, C. L. Fan, S. H. Wang and S. J. Wang, *Korean J. Chem. Eng.*, **26**, 1574 (2009).
23. H. Huang, S. H. Wang, S. J. Wang and G. P. Cao, *Catal. Lett.*, **134**, 351 (2010).
24. L. F. B. Lira, D. C. M. B. dos Santos, M. A. B. Guida, L. Stragevitch, M. G. A. Korn, M. F. Pimentel and A. P. S. Paim, *Fuel*, **90**, 3254 (2011).
25. R. Quinn, T. A. Dahl and B. A. Toseland, *Appl. Catal. A*, **272**, 61 (2004).
26. D. Z. Zhang, H. B. Yin, C. Ge, J. J. Xue, T. S. Jiang, L. B. Yu and Y. T. Shen, *J. Ind. Eng. Chem.*, **15**, 537 (2009).
27. D. Z. Zhang, H. B. Yin, R. C. Zhang, J. J. Xue and T. S. Jiang, *Catal. Lett.*, **122**, 176 (2008).
28. S. Velu, K. Suzuki, M. Vijayaraj, S. Barman and C. S. Gopinath, *Appl. Catal. B*, **55**, 287 (2005).
29. M. M. Waite and S. I. Shah, *Appl. Phys. Lett.*, **60**, 2344 (1992).
30. C. T. Campbell, K. A. Daube and J. M. White, *Surf. Sci.*, **182**, 458 (1987).
31. C. J. Vesely and D. W. Langer, *Phys. Rev. B*, **4**, 451 (1971).
32. NIST X-ray Photoelectron Spectroscopy Database, http://srdata.nist.gov/xps/.